Domain Reduction in Hybrid Technique for Electromagnetic Wave Scattering Problems

Malgorzata Warecka, Piotr Kowalczyk, Rafal Lech

Department of Microwave and Antenna Engineering,
Faculty of Electronics, Telecommunications and Informatics,
Gdansk University of Technology,
Narutowicza 11/12, 80-233 Gdansk, Poland,
e-mail: (see http://eti.pg.edu.pl/)

Abstract—This paper proposes a combination of the field matching technique, finite element method and generalized impedance matrix, the main idea of which is to reduce the computational domain by surrounding a scatterer with the smallest convex shape and applying the field matching technique. This approach can be applied for arbitrary shaped scatterers and types of materials and allows for the reduction of the computational domain. In order to verify the validity of the method, several examples have been investigated and compared with other numerical techniques.

Index Terms—finite element method, generalized impedance matrix, field matching method

I. INTRODUCTION

Scattering problems are very important in the context of design of microwave devices and their analysis. Many hybrid techniques were developed to combine advantages of analytical and discrete methods. One of the most popular hybrid methods is a combination of the finite element method (FEM) and the boundary integral equation [1]. In this approach a discretized domain is smaller than in FEM with a perfectly matched layer or transparent boundary conditions; however, it still requires the choice of appropriate current basis functions. It also necessitates the utilization of the Green's functions, which can be problematic due to their singularities. Another example can be a combination of the finite difference method and the mode matching technique [2], [3]. The mode matching approach itself is limited to only a few cases of simple geometries [4]–[6]. However, its great advantages are high accuracy and short computation time. On the other hand, the finite difference method is much more versatile and allows to investigate structures with complex geometries. Recently, another hybrid method was proposed, a combination of FEM, generalized impedance matrix (GIM) and mode matching (MM) technique [7]. This approach has all the advantages of the previous one and in contrast to the finite difference method it allows for easy inclusion of different types and shapes of materials because of the irregular mesh.
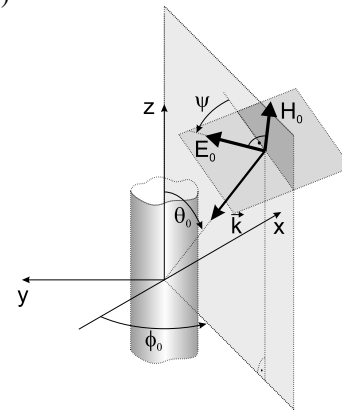
Fig. 1. Plane wave illumination at an arbitrary angle.

In this paper a hybrid method that is a combination of FEM, GIM and field matching (FM) technique [8] is presented. Utilization of FM instead of MM is significant in a context of domain reduction. The computational domain is divided into two regions: the first one, where FEM is utilized, and the second one, where field matching technique is applied. The utilization of FM technique allows for a reduction of the inner region to any convex shape. Such approach can reduce the discrete part of the computational domain more than a combination proposed in [7] (where only a circular shape of inner region is possible). Two different examples of scatterers are investigated and the results are verified.

II. FORMULATION OF THE PROBLEM

The investigated structure is illuminated by a plane wave at an arbitrary angle (see Fig.1). Let us assume that an obstacle is infinite and homogeneous in one direction, therefore the problem is reduced to a 2.5D case. The structure has an arbitrary cross section and can be anisotropic. The aim of the analysis is to calculate the scattered field at any distance. In the presented approach the computational domain is divided into two regions. The inner one is limited by any convex geometrical shape - see Fig. 2. If the cross section of the obstacle is convex, its contour can be set as the boundary of region I. In this region FEM is utilized and the GIM is

obtained. The outer region is not discretized and the fields can be expressed as series of Bessel and Hankel functions:

$$E_z^{II}(\rho,\varphi,z) = \tag{1}$$
$$\sum_{m=-M}^{M}\left(a_m^E J_m(k_\rho\rho) + b_m^E H_m^{(2)}(k_\rho\rho)\right)e^{jm\varphi}e^{jk_z z},$$

and

$$H_z^{II}(\rho,\varphi,z) = \tag{2}$$
$$\sum_{m=-M}^{M}\left(a_m^H J_m(k_\rho\rho) + b_m^H H_m^{(2)}(k_\rho\rho)\right)e^{jm\varphi}e^{jk_z z},$$

where $k_\rho = (\omega^2\mu_0\varepsilon_0 - k_z^2)^{1/2}$, $k_z = k_0\cos\theta_0$, k_0 is a wavenumber of free space, a_m^E, a_m^H are the coefficients of the incident wave and b_m^E, b_m^H are the coefficients of the scattered field.

In order to use GIM to analyze fields in the inner region, the tangential components of the electric and magnetic fields at the boundary must be expressed with the use of fixed basis functions. It requires the introduction of a new curvilinear coordinate s that follows the boundary and changes from 0 to the total length S (the circumference of the inner region). The tangential components of the fields at the boundary can be described as follows:

$$\vec{E}_z(\rho(s),\varphi(s),z) = \sum_{m=-M}^{M} V_{zm}\vec{e}_{zm}(\rho(s),\varphi(s),z), \tag{3}$$

$$\vec{E}_t(\rho(s),\varphi(s),z) = \sum_{m=-M}^{M} V_{tm}\vec{e}_{tm}(\rho(s),\varphi(s),z), \tag{4}$$

$$\vec{H}_t(\rho(s),\varphi(s),z) = \sum_{m=-M}^{M} I_{tm}\vec{h}_{tm}(\rho(s),\varphi(s),z), \tag{5}$$

$$\vec{H}_z(\rho(s),\varphi(s),z) = \sum_{m=-M}^{M} I_{zm}\vec{h}_{zm}(\rho(s),\varphi(s),z), \tag{6}$$

where $V_{zm}, V_{tm}, I_{tm}, I_{zm}$ are the coefficients of the fields and $\vec{e}_{zm},\vec{e}_{tm},\vec{h}_{tm},\vec{h}_{zm}$ are the expansion functions. The transversal component of these fields can be written as a linear combination of two components:

$$\vec{e}_{tm}(\rho(s),\varphi(s),z) = C_\rho(s)\vec{e}_{\rho m}(s,z) + C_\varphi(s)\vec{e}_{\varphi m}(s,z), \tag{7}$$

$$\vec{h}_{tm}(\rho(s),\varphi(s),z) = C_\rho(s)\vec{h}_{\rho m}(s,z) + C_\varphi(s)\vec{h}_{\varphi m}(s,z), \tag{8}$$

where the coefficients have the following form:

$$C_\rho(s) = \sin\varphi(s)\cos\alpha(s) - \cos\varphi(s)\sin\alpha(s), \tag{9}$$
$$C_\varphi(s) = \cos\varphi(s)\cos\alpha(s) + \sin\varphi(s)\sin\alpha(s) \tag{10}$$

and angles $\alpha(s)$ and $\varphi(s)$ are defined in Fig. 2. The expansion functions introduced in (3)-(6) can be chosen arbitrarily. In this paper an orthogonal set of functions proposed in [7] is assumed:

$$\begin{aligned}\vec{e}_{\rho m}(s,z) &= -w_m(s,z)\vec{i}_\rho, & \vec{h}_{\rho m}(s,z) &= w_m(s,z)\vec{i}_\rho,\\ \vec{e}_{\varphi m}(s,z) &= -w_m(s,z)\vec{i}_\varphi, & \vec{h}_{\varphi m}(s,z) &= w_m(s,z)\vec{i}_\varphi, \\ \vec{e}_{zm}(s,z) &= w_m(s,z)\vec{i}_z, & \vec{h}_{zm}(s,z) &= w_m(s,z)\vec{i}_z,\end{aligned} \tag{11}$$
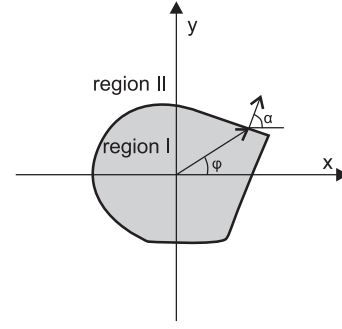

Fig. 2. Cross section of the obstacle.

where

$$w_m(s,z) = \frac{1}{\sqrt{S}}\exp\left(\frac{j2\pi m}{S}s\right)\exp\left(jk_z z\right). \tag{12}$$

To fulfill the continuity conditions at the boundary the following projection is applied:

$$\begin{aligned}\left\langle \vec{E}_z^I(\rho(s),\varphi(s),z)|\vec{e}_z\right\rangle &= \left\langle \vec{E}_z^{II}(\rho(s),\varphi(s),z)|\vec{e}_{zp}\right\rangle,\\ \left\langle \vec{E}_t^I(\rho(s),\varphi(s),z)|\vec{e}_t\right\rangle &= \left\langle \vec{E}_t^{II}(\rho(s),\varphi(s),z)|\vec{e}_{tp}\right\rangle,\\ \left\langle \vec{H}_z^I(\rho(s),\varphi(s),z)|\vec{h}_z\right\rangle &= \left\langle \vec{H}_z^{II}(\rho(s),\varphi(s),z)|\vec{h}_{zp}\right\rangle,\\ \left\langle \vec{H}_t^I(\rho(s),\varphi(s),z)|\vec{h}_t\right\rangle &= \left\langle \vec{H}_t^{II}(\rho(s),\varphi(s),z)|\vec{h}_{tp}\right\rangle,\end{aligned}$$

where $z\in\mathbb{R}$ and the inner product is defined as follows:

$$< \vec{g}|\vec{f}_p> = \int_0^S \vec{g}(s)\circ\vec{f}_p(s)^*\,ds. \tag{13}$$

Since the set of functions (12) is orthonormal, the field coefficients satisfy the system of equations:

$$\mathbf{V} = \mathbf{M}_A^E\mathbf{a} + \mathbf{M}_B^E\mathbf{b}, \tag{14}$$
$$\mathbf{I} = \mathbf{M}_A^H\mathbf{a} + \mathbf{M}_B^H\mathbf{b}, \tag{15}$$

where $\mathbf{a} = [\mathbf{a}^E, \mathbf{a}^H]^T$, $\mathbf{b} = [\mathbf{b}^E, \mathbf{b}^H]^T$, $\mathbf{V} = [\mathbf{V}_z, \mathbf{V}_t]^T$ and $\mathbf{I} = [\mathbf{I}_t, \mathbf{I}_z]^T$ and the matrices take the forms:

$$\mathbf{M}_l^H = \begin{bmatrix}\mathbf{M}_{l,t1}^H & \mathbf{M}_{l,t2}^H\\ 0 & \mathbf{M}_{l,z}^H\end{bmatrix}, \quad \mathbf{M}_l^E = \begin{bmatrix}\mathbf{M}_{l,z}^E & 0\\ \mathbf{M}_{l,t1}^E & \mathbf{M}_{l,t2}^E\end{bmatrix} \tag{16}$$

$l \in \{A, B\}$. All the submatrices are projections on the orthogonal set of functions:

$$\begin{aligned}\{\mathbf{M}_{A,z}^E\}_p^m &= \left\langle J_m(k_\rho\rho)e^{jm\varphi}\vec{i}_z|\vec{e}_{zp}\right\rangle,\\ \{\mathbf{M}_{B,z}^E\}_p^m &= \left\langle H_m^{(2)}(k_\rho\rho)e^{jm\varphi}\vec{i}_z|\vec{e}_{zp}\right\rangle,\\ \{\mathbf{M}_{A,z}^H\}_p^m &= \left\langle J_m(k_\rho\rho)e^{jm\varphi}\vec{i}_z|\vec{h}_{zp}\right\rangle,\\ \{\mathbf{M}_{B,z}^H\}_p^m &= \left\langle H_m^{(2)}(k_\rho\rho)e^{jm\varphi}\vec{i}_z|\vec{h}_{zp}\right\rangle,\end{aligned}$$

$$\{\mathbf{M}_{A,t1}^E\}_p^m = \left\langle C_\rho^{E,e} J_m'(k_\rho\rho)\vec{i}_\rho + C_\varphi^{E,e} J_m(k_\rho\rho)\vec{i}_\varphi | \vec{e}_{tp} \right\rangle,$$

$$\{\mathbf{M}_{B,t1}^E\}_p^m = \left\langle C_\rho^{E,e} H_m'^{(2)}(k_\rho\rho)\vec{i}_\rho + C_\varphi^{E,e} H_m^{(2)}(k_\rho\rho)\vec{i}_\varphi | \vec{e}_{tp} \right\rangle,$$

$$\{\mathbf{M}_{A,t2}^E\}_p^m = \left\langle C_\rho^{E,h} J_m(k_\rho\rho)\vec{i}_\rho + C_\varphi^{E,h} J_m'(k_\rho\rho)\vec{i}_\varphi | \vec{e}_{tp} \right\rangle,$$

$$\{\mathbf{M}_{B,t2}^E\}_p^m = \left\langle C_\rho^{E,h} H_m^{(2)}(k_\rho\rho)\vec{i}_\rho + C_\varphi^{E,h} H_m'^{(2)}(k_\rho\rho)\vec{i}_\varphi | \vec{e}_{tp} \right\rangle,$$

$$\{\mathbf{M}_{A,t1}^H\}_p^m = \left\langle C_\rho^{H,e} J_m(k_\rho\rho)\vec{i}_\rho + C_\varphi^{H,e} J_m'(k_\rho\rho)\vec{i}_\varphi | \vec{h}_{tp} \right\rangle,$$

$$\{\mathbf{M}_{B,t1}^H\}_p^m = \left\langle C_\rho^{H,e} H_m^{(2)}(k_\rho\rho)\vec{i}_\rho + C_\varphi^{H,e} H_m'^{(2)}(k_\rho\rho)\vec{i}_\varphi | \vec{h}_{tp} \right\rangle,$$

$$\{\mathbf{M}_{A,t2}^H\}_p^m = \left\langle C_\rho^{H,h} J_m'(k_\rho\rho)\vec{i}_\rho + C_\varphi^{H,h} J_m(k_\rho\rho)\vec{i}_\varphi | \vec{h}_{tp} \right\rangle,$$

$$\{\mathbf{M}_{B,t2}^H\}_p^m = \left\langle C_\rho^{H,h} H_m'^{(2)}(k_\rho\rho)\vec{i}_\rho + C_\varphi^{H,h} H_m^{(2)}(k_\rho\rho)\vec{i}_\varphi | \vec{h}_{tp} \right\rangle,$$

where

$$C_\rho^{E,e} = \frac{\mathrm{j}k_z}{k_\rho}C_\rho e^{\mathrm{j}m\varphi}, \qquad C_\varphi^{E,e} = \frac{-k_z m}{k_\rho^2\rho}C_\varphi e^{\mathrm{j}m\varphi},$$

$$C_\rho^{E,h} = \frac{\omega\mu m}{k_\rho^2\rho}C_\rho e^{\mathrm{j}m\varphi}, \qquad C_\varphi^{E,h} = \frac{\mathrm{j}\omega\mu}{k_\rho}C_\varphi e^{\mathrm{j}m\varphi},$$

$$C_\rho^{H,e} = \frac{-\omega\varepsilon m}{k_\rho^2\rho}C_\rho e^{\mathrm{j}m\varphi}, \qquad C_\varphi^{H,e} = \frac{-\mathrm{j}\omega\varepsilon}{k_\rho}C_\varphi e^{\mathrm{j}m\varphi},$$

$$C_\rho^{H,h} = \frac{\mathrm{j}k_z}{k_\rho}C_\rho e^{\mathrm{j}m\varphi}, \qquad C_\varphi^{H,h} = \frac{-k_z m}{k_\rho^2\rho}C_\varphi e^{\mathrm{j}m\varphi}.$$

The GIM is a relation between coefficients of electric and magnetic fields on the boundary

$$\begin{bmatrix} \mathbf{V}_z \\ \mathbf{V}_t \end{bmatrix} = \mathbf{Z} \begin{bmatrix} \mathbf{I}_t \\ \mathbf{I}_z \end{bmatrix} = \begin{bmatrix} \mathbf{Z}_{TM,TM} & \mathbf{Z}_{TM,TE} \\ \mathbf{Z}_{TE,TM} & \mathbf{Z}_{TE,TE} \end{bmatrix} \begin{bmatrix} \mathbf{I}_t \\ \mathbf{I}_z \end{bmatrix}. \qquad (17)$$

Applying the definition of the GIM to the equations (14) and (15), the following relation can be obtained:

$$\mathbf{b} = (\mathbf{M}_B^E - \mathbf{Z}\mathbf{M}_B^H)^{-1}(\mathbf{Z}\mathbf{M}_A^H - \mathbf{M}_A^E)\mathbf{a}. \qquad (18)$$

This relation combines the incident field (represented by coefficients $\mathbf{a}$) with the scattered one (represented by coefficients $\mathbf{b}$). It can be applied for analysis of any type of incident wave and any structures located inside the inner region. However, this relation involves GIM defined for the inner region, which in general cannot be found analytically. The aforementioned GIM can be obtained using the FEM, as it is described in details in [7]. The final formula of the GIM can be expressed as

$$\mathbf{Z} = \mathbf{B}^H \mathbf{G}^{-1} \mathbf{B} \qquad (19)$$

where the $\mathbf{G}$ matrix is defined in previous papers [7], [9] and only elements of $\mathbf{B}$ matrix require a modification according to the following formulas:

$$\left[\mathbf{B}_z^{[n]}\right]_{p,m} = \mathrm{j}\omega\mu_0 \int_{L\cap L^{[n]}} \vec{W}_{(p)}^{[n]} \circ (\vec{n} \times \vec{h}_{zm})\, dl,$$

$$\left[\mathbf{B}_\varphi^{[n]}\right]_{p,m} = \mathrm{j}\omega\mu_0 \int_{L\cap L^{[n]}} \vec{\alpha}_{(p)}^{[n]} \circ (\vec{n} \times \vec{h}_{tm})\, dl,$$

where $\vec{n} = [\cos\alpha, \sin\alpha, 0]$ is a surface normal vector for each point. In opposite to [7], since

$$\int_L \vec{E}_t \circ (\vec{n} \times \vec{h}_{zm})^*\, dl \qquad (20)$$

$$= \sum_{p=-M}^M V_{tp} \int_L \vec{e}_{tp} \circ (\vec{n} \times \vec{h}_{zm})^*\, dl = V_{tm},$$

$$\int_L E_z\vec{i}_z \circ (\vec{n} \times \vec{h}_{tm})^*\, dl \qquad (21)$$

$$= \sum_{p=-M}^M V_{zp} \int_L \vec{e}_{zp} \circ (\vec{n} \times \vec{h}_{tm})^*\, dl = V_{zm},$$

Δ matrix in [7] is an eye matrix.

III. NUMERICAL RESULTS

In order to confirm the validity of the presented approach two examples of obstacles are investigated. The analyses are performed at frequency 10 GHz, for an incident wave, which illuminates at the angle $\theta_0 = 30°$, $\phi_0 = 30°$ and $\psi = 30°$.

Firstly, a multilayered obstacle is presented. The structure contains two layers: the first (inner) one is of a triangular shape with relative permittivity $\varepsilon_r = 5$ and the second one is a rectangular shape with relative permittivity $\varepsilon_r = 2$, as presented in Fig. 3. The structure has the following dimensions: $a = \lambda_0$, $b = 0.5\lambda_0$, $R = \lambda_0/40$, $d = \lambda_0/2$ and $r = \lambda_0/40$. In this case the computational domain is limited to the edge of the outer layer, due to its convex shape. The results are compared with the ones obtained with the use of FM method and presented in [10] (dashed lines); a good agreement is achieved.

The second example is a dielectric ridge guide shown in Fig. 4 with dimensions $e = 0.5\lambda_0$, $f = 2\lambda_0$, $d = 0.5\lambda_0$ and $h = 0.25\lambda_0$ and relative permittivity $\varepsilon_r = 4$. Since the investigated structure is concave, the ridge is surrounded by an artificial rectangle with rounded corners with relative permittivity $\varepsilon_r = 1$ and dimensions $a = 0.6\lambda_0$, $b = 2.1\lambda_0$ and $R = 0.06\lambda_0$. The results are compared with the ones obtained using technique described in [7]. The number of elements in this approach is 5054, while in a compared method 6260.
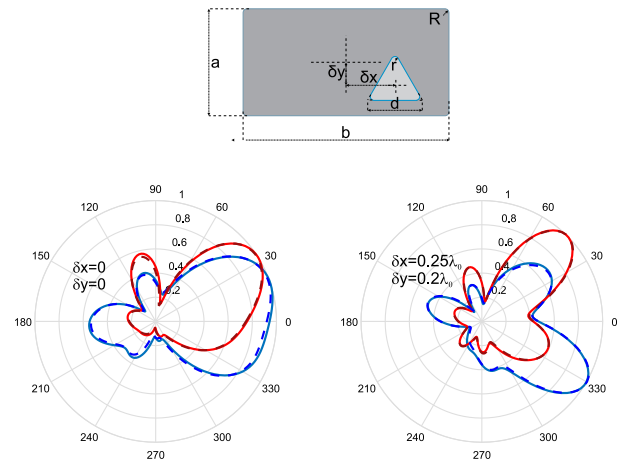

Fig. 3. Normalized amplitude of scattered electric (blue) and magnetic (red) fields from the dielectric rectangular-triangular post.
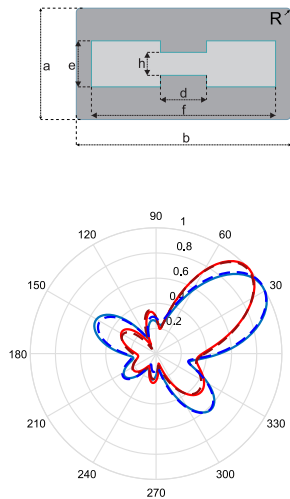
Fig. 4. Normalized amplitude of scattered electric (blue) and magnetic (red) fields from the dielectric ridge.

In both analyses the density of the mesh is similar and the maximum length of triangle edge is the same and the results are compatible. The efficiency of the method increases with elongation of the scatterer cross-section (for structures with similar cross-sectional dimensions should not be applied).

IV. CONCLUSION

A combination of FEM, GIM and field matching method was presented. The validity of the approach has been verified for two different cases. A multilayered and a concave structures was investigated and a good agreement with other numerical techniques has been obtained. This approach allows for reduction of variables in the analysis, due to limitation of the computational domain.

REFERENCES

[1] X.-Q. Sheng, J.-M. Jin, J. Song, C.-C. Lu, and W. C. Chew, "On the formulation of hybrid finite-element and boundary-integral methods for 3-D scattering," *IEEE Transactions on Antennas and Propagation*, vol. 46, no. 3, pp. 303–311, 1998.

[2] A. Kusiek, R. Lech, and J. Mazur, "A new hybrid method for analysis of scattering from arbitrary configuration of cylindrical objects," *IEEE transactions on antennas and propagation*, vol. 56, no. 6, pp. 1725–1733, 2008.

[3] A. Kusiek and J. Mazur, "Application of hybrid finite-difference mode-matching method to analysis of structures loaded with axially symmetrical posts," *Microwave and Optical Technology Letters*, vol. 53, no. 1, pp. 189–194, 2011.

[4] J. Kong, L. Tsang, and K. Ding, "Scattering of electromagnetic waves, theories and applications, vol. 1," 2000.

[5] A. Elsherbeni, M. Hamid, and G. Tian, "Iterative scattering of a gaussian beam by an array of circular conducting and dielectric cylinders," *Journal of Electromagnetic Waves and Applications*, vol. 7, no. 10, pp. 1323–1342, 1993.

[6] E. Nielsen, "Scattering by a cylindrical post of complex permittivity in a waveguide," *IEEE Transactions on Microwave Theory and Techniques*, vol. 17, no. 3, pp. 148–153, 1969.

[7] P. Kowalczyk, R. Lech, M. Warecka, and A. Kusiek, "Electromagnetic plane wave scattering from a cylindrical object with an arbitrary cross section using a hybrid technique," *Journal of Electromagnetic Waves and Applications*, pp. 1–15, 2018.

[8] R. Lech, P. Kowalczyk, and A. Kusiek, "Scattering from a cylindrical object of arbitrary cross section with the use of field matching method," *IEEE Transactions on Antennas and Propagation*, vol. 64, no. 11, pp. 4883–4887, 2016.

[9] M. Warecka, R. Lech, and P. Kowalczyk, "Efficient finite element analysis of axially symmetrical waveguides and waveguide discontinuities," *IEEE Transactions on Microwave Theory and Techniques*, vol. 67, no. 11, pp. 4291–4297, Nov 2019.

[10] ——, "Scattering and propagation analysis for the multilayered structures based on field matching technique," in *2019 13th European Conference on Antennas and Propagation (EuCAP)*, March 2019, pp. 1–4.